Study of Belle II detector performance with τ lepton decays

Paul Feichtinger, TU Wien, Austria

supervised by

Ilya Komarov, Armine Rostomyan,

Francesco Tenchini, Petar Kevin Rados

September 4, 2019

Abstract

This reports gives an overview over my project as part of the Summer Student program at DESY. I worked with the Belle II tau group on events with 3-prong and 1-prong tau decays, measuring the branching fractions of the decay $\tau \to \mu\nu_\mu\nu_\tau$ and $\tau \to \pi\nu_\tau$ in order to understand detector performance. This project was part of a complementary study involving three other students with the goal to take ratios of branching fractions for different decays. Thereby some common detector efficiencies cancel and we get an estimate for other detector properties by comparing our result to the measured values listed in the PDG.

Contents

1 Introduction

1.1 Belle II

The Belle II experiment located in Tsukuba, Japan, collides electrons and positrons with a center of mass energy of $\sqrt{s} = 10.58\,\text{GeV}$ which is the mass of the $\Upsilon(4S)$ resonance. It is considered to be a precision experiment since it is not looking for new Physics at higher energies, but rather probes our current understanding of Physics processes with high precision. This is possible because of the high luminosity provided by the Super KEKB accelerator.

Besides being a B factory, Belle II is also a τ factory since the process $e^+e^- \to \tau^+\tau^-$ has a relatively large cross section. This, together with the clean collisions and possibility of full event reconstruction Belle II can be used for the study of τ lepton decays.

In Figure 1 the Belle II detector with its main components can be seen. Most important for this analysis are the central drift chamber (CDC) which provides tracking information, the electromagnetic calorimeter (ECL) where charged particles and photons deposit energy, and the KL and muon detector (KLM) which detects long lived massive particles that passed through the inner detector ($\mu^\pm$, K^0_L as well as $\pi^\pm$ and protons).

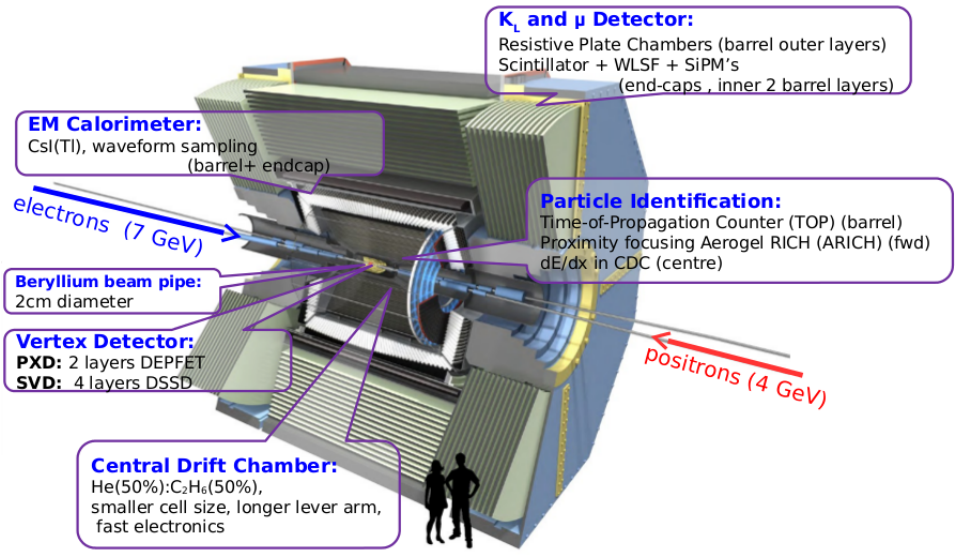

Figure 1: The Belle II detector.

1.2 τ decays

This projects main goal is to calculate branching fractions for the decays $\tau \to \mu\nu_\mu\nu_\tau$ and $\tau \to \pi\nu_\tau$. In Figure 2 a Feynman diagram corresponding to these decays is shown. The reason why I will look at both decays is because μ and π separation is not well calibrated in the current state of the detector and this study can serve as a validation

for particle identification. In the future a look at these decays can serve as a test for the standard model.

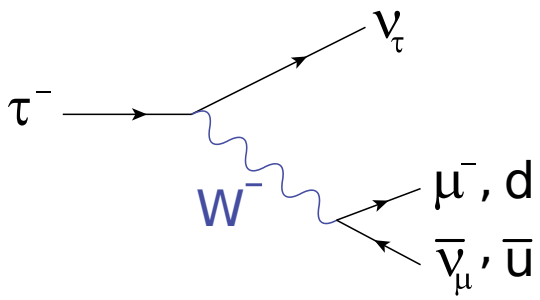

Figure 2: The Feynman diagram corresponding to $\tau \to \mu\nu_\mu\nu_\tau$

The τ we will use for this analysis originates from the process $e^+e^- \to \tau^+\tau^-$. Tau leptons can decay either into one charged particle which is called 1-prong decay, or 3 charged particles which is called 3-prong decay. The τ that decays into (μ ν_μ ν_τ) or (π ν_τ) will be called τ_{sig}. For the tag side we select τ leptons that decay to 3-prong, because this increases our trigger efficiency and the resulting event shape is expected to have low background. A event like this is sketched in Figure 3.

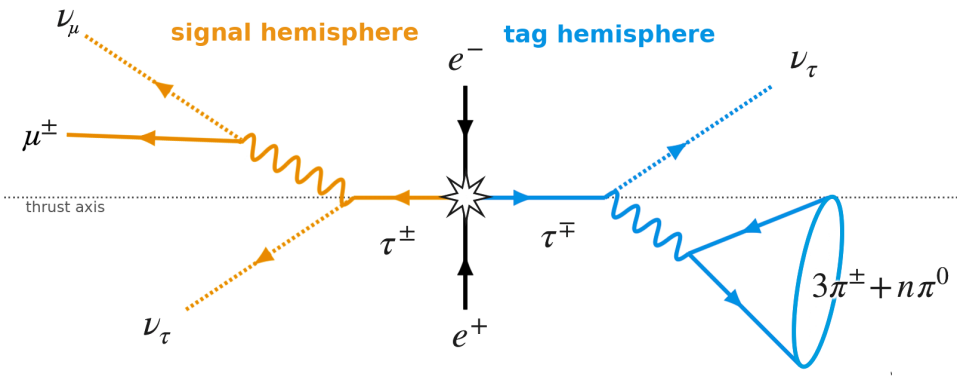

Figure 3: $e^+e^- \to \tau^+\tau^-$ with one τ decaying via 1-prong and the other via 3-prong.

2 Data and MC samples

2.1 Data

We used data collected at Belle II in the spring and summer of 2019, which is split into Experiment 7 (Exp7) and Experiment 8 (Exp8). The samples we used have a total integrated luminosity of $(1982.3 \pm 0.6)\,\text{pb}^{-1}$ for Exp8 and $(642.8 \pm 0.3)\,\text{pb}^{-1}$ for Exp7

which was obtained using Bhabha events as a reference. All calculations in this report were done only with Exp8.

2.2 Monte Carlo

We used Monte Carlo simulations including onefold beam background to identify our signal and background. The simulated processes with their respective cross sections, total number of events and the corresponding luminosities are listed in Table 1. The different processes are scaled to data luminosity accordingly. The scale factor for to the luminosity of exp8 can also be found in Table 1.

Process	Events [$\times 10^6$]	cross section [nb]	Luminosity [fb^{-1}]	scale factor
$ee \to \tau\tau$	73.52	0.919	80	0.0248
$ee \to ee(\gamma)$	50	300 ± 3	0.1667	11.8938
$ee \to \pi\pi$ ISR	200	0.16759 ± 0.00015	1193.39	0.0017
$ee \to eeee$	210.6	39.7 ± 0.1	5.3048	0.3737
$ee \to ee\mu\mu$	100	18.9 ± 0.1	5.291	0.3747
$ee \to \mu\mu(\gamma)$	55	1.148	47.9094	0.0414
$ee \to d\bar{d}$	32.08	0.4	80	0.0248
$ee \to c\bar{c}$	106.32	1.3	69.92	0.0284
$ee \to u\bar{u}$	128.4	1.61	80	0.0248
$ee \to s\bar{s}$	30.64	0.38	80	0.0248

Table 1: Simulated processes from Monte Carlo.

3 Event selections

3.1 Candidate event selection

For our analysis we reconstruct photons with an energy greater than 200 MeV and π^0 using a threshold on photon energy of 100 MeV. For reconstruction of τ we select events with four good tracks in the detector whose origin does not deviate more than 2 cm from the interaction point (IP) in radial direction and not more than 5 cm in z direction. No further tracks that satisfy this condition are allowed. One track is required to be in one hemisphere and the other three in the other hemisphere of the event and they are required to have zero net charge. The hemispheres are defined using the thrust axis $\hat{t}$ of the event, defined by maximizing the thrust value

$$V_{thrust} \overset{max}{=} \sum_i \frac{|\vec{p}_i \cdot \hat{t}|}{\sum_j |\vec{p}_j|}, \tag{1}$$

where $\vec{p}_j$ is the momentum in the CMS and the sums are over all particles and photons visible in the event. The plane normal to the thrust vector is used to separate the hemispheres.

In order to reject electrons and positrons all tracks are required to have $E_{\text{cluster}}/p_{\text{lab}} < 0.8$ where p_{lab} is the momentum of the particle in the laboratory frame and E_{cluster} is the total energy deposited in the electromagnetic calorimeter. A distribution of $E_{\text{cluster}}/p_{\text{lab}}$ for the track on the 1-prong side can be seen in Figure 4 for μ, π and e. We also reject events where at least one track can not be matched to an energy deposit in the ECL. This is in order to suppress background processes where tracks have low transverse momentum and do not reach the ECL.

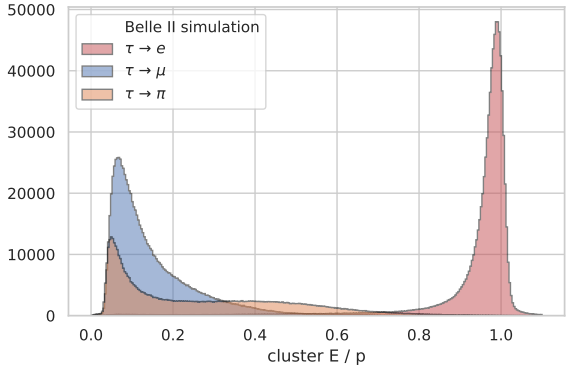

Figure 4: The distribution of the deposited energy in the ECL divided by the particle momentum is used for particle identification.

3.2 Background suppression

3.2.1 Important variables

The thrust value can be thought of as the sphericity of the event, with a value corresponding to 0.5 being a maximal spherical event while a value close to one describes an event where all tracks are aligned with the thrust axis. In Figure 5a the thrust value of signal and background distributions overlaid with data are shown. Because the relevant τ lepton decays on the 1-prong side deviate not far from the primary trajectory we can apply a lower cut on thrust in order to get rid of some $q\bar{q}$ background. Also an upper cut on thrust will remove some background coming from $ee \to ee(\gamma)$. This process is known as Bhabha scattering and it has by far the largest cross section (see Table 1). However, most of these events are already removed by the candidate selections ($E_{\text{cluster}}/p < 0.8$ and E_{cluster} != NaN).

Another important variable is the total visible energy of the event in the center of mass system. Since there are undetected neutrinos in the signal events the distribution of our signal is expected to be shifted to lower values than the collision energy $\sqrt{s}$. Other background processes will peak at $\sqrt{s}$. The distributions can be seen in Figure 5b.

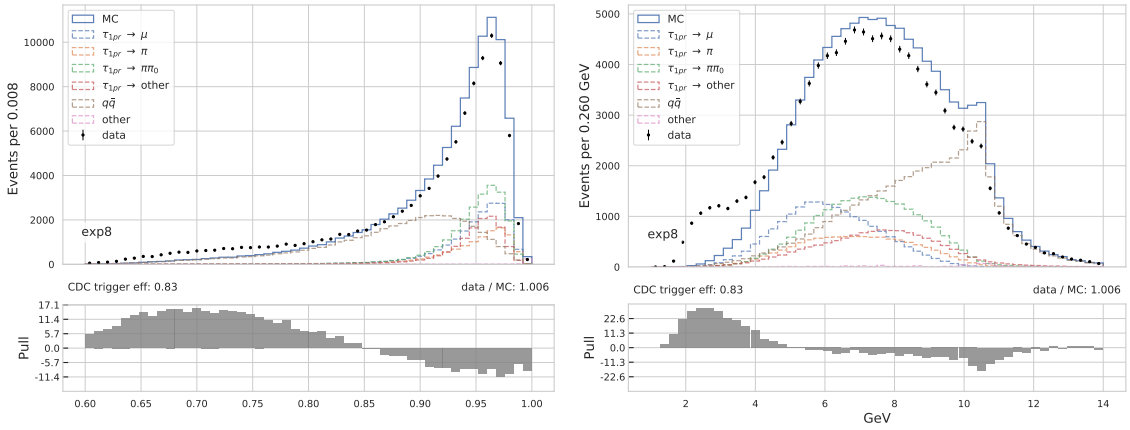

(a) thrust value

(b) visible energy of Event (CMS)

Figure 5: Distributions for thrust and visible energy for different processes and comparison between data and MC.

3.2.2 Purity, signal efficiency and FOM

For the branching fraction calculation uncertainties can be reduced by selecting subsamples in order to maximize the contribution of the desired decaychannel. To quantify this we define the signal purity

$$p = \frac{N_{\mathsf{sig}}}{N_{\mathsf{sig}} + N_{\mathsf{bkg}}}. \tag{2}$$

Here N_{sig} is the total number of signal events in MC and N_{bkg} is the total number of background events in MC. Another quantity of importance is the signal efficiency,

$$\epsilon_{\mathsf{sig}} = \frac{N_{\mathsf{sig}}}{2\mathcal{B}_{\mathsf{sig}}\mathcal{B}_{\mathsf{tag}}N_{\mathsf{gen}}}, \tag{3}$$

where N_{gen} stands for the total number of events that were generated in the MC sample. Because this sample ($ee \to \tau\tau$) includes all τ decays we still need to multiply this number by the branching fractions of our signal (1-prong side, $\hat{\mathcal{B}}_{\mathsf{sig}}$) and by the branching fraction of the inclusive 3-prong decay ($\hat{\mathcal{B}}_{\mathsf{tag}}$). $\hat{\mathcal{B}}_{\mathsf{sig}}$ and $\hat{\mathcal{B}}_{\mathsf{tag}}$ are the branching fractions that were used for the generation of the events. For my calculations I will use the values listed in Table 2 taken from the PDG. The factor of 2 is included because the 1-prong / 3-prong decay can originate either from τ^- or τ^+.

Some cuts for my samples are chosen in order to maximize the figure of merit (FOM) defined by

$$\sqrt{p \ \cdot \ N_{sig}}. \tag{4}$$

This quantity is chosen because in general one wants to maximize purity of the samples while not loosing too much signal events in doing so. By maximizing the FOM both are taken into account. The FOM was used to optimize the cuts on visible energy and cluster energy for my samples. In Figure 6 the MC signal and backgrounds for both

τ^- Decay Mode	$\hat{\mathcal{B}}$
$h^-h^-h^+ \geq 0$ neutrals $\geq 0 K_L^0 \nu_\tau$	$(15.20 \pm 0.06)\%$
$\mu^- \overline{\nu}_\mu \nu_\tau$	$(17.39 \pm 0.04)\%$
$\pi^- \nu_\tau$	$(10.82 \pm 0.05)\%$

Table 2: Branching fractions taken from PDG.

selection	signal eff.	purity
after preselection	$(22.66 \pm 0.11)\,\%$	$(17.23 \pm 0.02)\,\%$
$N^{\pi^0}_{\text{1prong}} < 1$	$(22.52 \pm 0.11)\,\%$	$(31.40 \pm 0.04)\,\%$
$N^{\gamma}_{\text{1prong}} < 1$	$(21.05 \pm 0.10)\,\%$	$(49.14 \pm 0.09)\,\%$
$0.91 <$ thrust < 0.99	$(18.74 \pm 0.09)\,\%$	$(54.51 \pm 0.04)\,\%$
$E^{cluster}_{\text{1prong}} < 0.336$	$(18.45 \pm 0.09)\,\%$	$(66.67 \pm 0.05)\,\%$
$E^{visible}_{\text{CMS}} < 9.408$	$(18.24 \pm 0.09)\,\%$	$(68.78 \pm 0.05)\,\%$

Table 3: Applied cuts for μ sample.

samples are shown together with purity and the FOM as a function of the upper cut on visible energy in the CMS.

3.2.3 Applied selections

The selections that were used to suppress background for $\tau \to \mu\nu_\mu\nu_\tau$ and $\tau \to \pi\nu_\tau$ are listed in Table 3 and Table 4 respectively, together with the resulting signal efficiencies and purities after each cut.

The requirement for no π^0 on the 1-prong side is aimed to suppress $\tau_{\text{1prong}} \to \pi\pi^0\nu_\tau$. Because of low π^0 and γ reconstruction efficiency sometimes just one photon originating from a π^0 is reconstructed and we also require no photons on the 1-prong side. These selections also reduce a lot of $\tau\tau \to q\bar{q}$ background. The selection on thrust is chosen to reduce background mentioned in Section 3.2.1 but also to cut away the large data / MC discrepancies at low thrust and visible energy (see Figure 5). Selections on $E^{cluster}_{\text{1prong}}$ and $E^{visible}_{\text{CMS}}$ were chosen by maximizing the FOM introduced it Section 3.2.2.

The purity after all cuts for the μ enriched sample is 69 % and for the π enriched sample it is 28 %. Due to the absence of π/ μ separation especially in the pion sample the signal fraction is quite low. In Figure 7 the signal and background contributions from MC overlaid with data is shown for thrust and visible energy in the CMS after the applied selections.

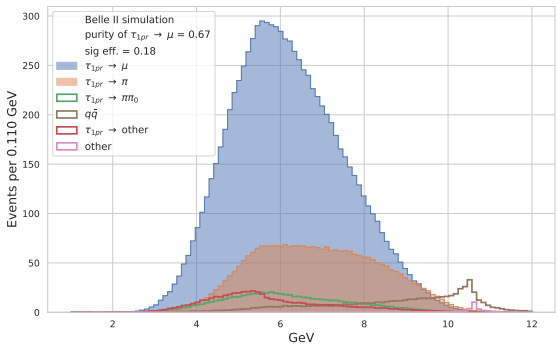

(a) Background distributions for visible energy in the CMS for the μ sample.

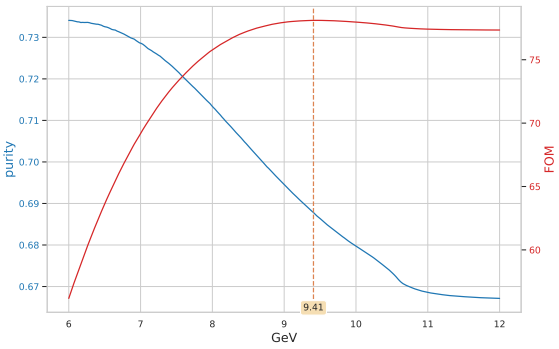

(b) The FOM and purity as a function of the cut value for the μ sample.

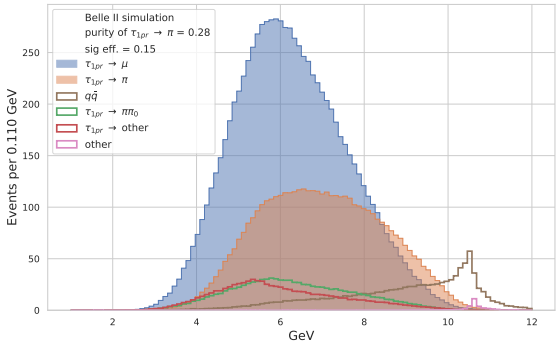

(c) Background distributions for visible energy in the CMS for the π sample.

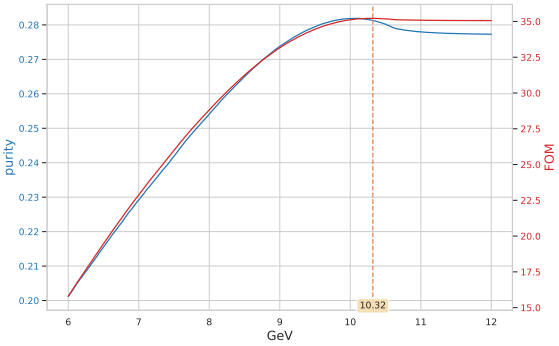

(d) The FOM and purity as a function of the cut value for the π sample.

Figure 6: Using a FOM to optimize the cut value.

selection	signal eff.	purity
after preselection	$(21.92 \pm 0.14)\,\%$	$(10.37 \pm 0.01)\,\%$
$N^{\pi^0}_{\text{1prong}} < 1$	$(21.50 \pm 0.13)\,\%$	$(18.64 \pm 0.03)\,\%$
$N^{\gamma}_{\text{1prong}} < 1$	$(17.32 \pm 0.11)\,\%$	$(25.15 \pm 0.05)\,\%$
$0.91 < \text{thrust} < 0.99$	$(14.97 \pm 0.09)\,\%$	$(27.11 \pm 0.04)\,\%$
$E^{cluster}_{\text{1prong}} > 0.144$	$(14.66 \pm 0.09)\,\%$	$(27.71 \pm 0.04)\,\%$
$E^{visible}_{\text{CMS}} < 10.32$	$(14.58 \pm 0.09)\,\%$	$(28.13 \pm 0.04)\,\%$

Table 4: Applied cuts for π sample.

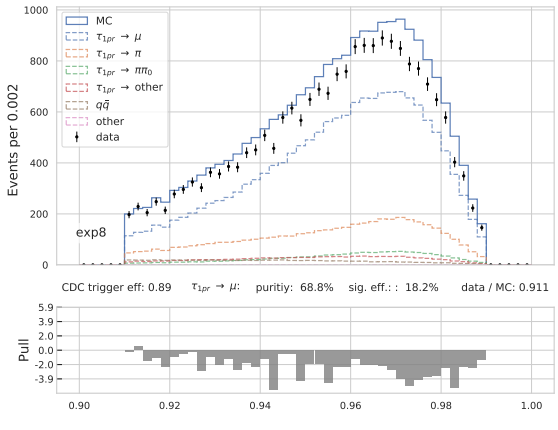

(a) thrust (μ enriched sample)

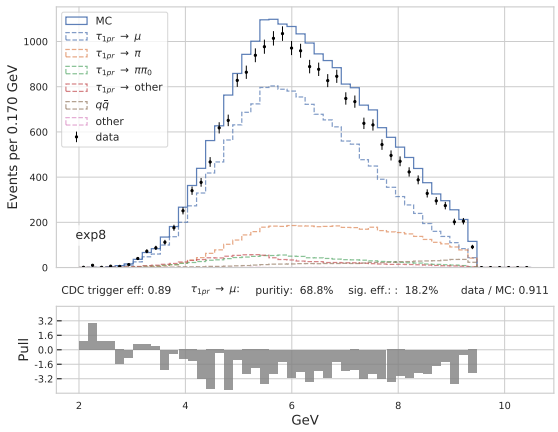

(b) visible energy CMS (μ enriched sample)

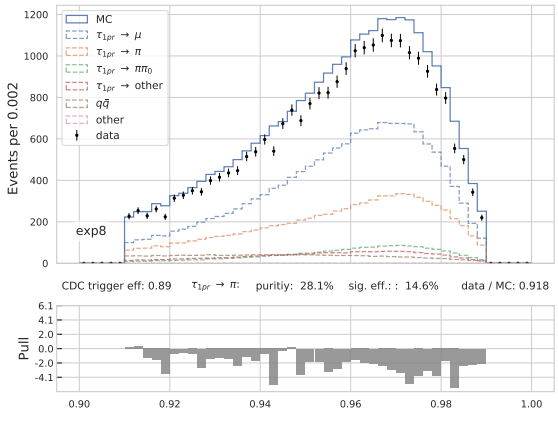

(c) thrust (π enriched sample)

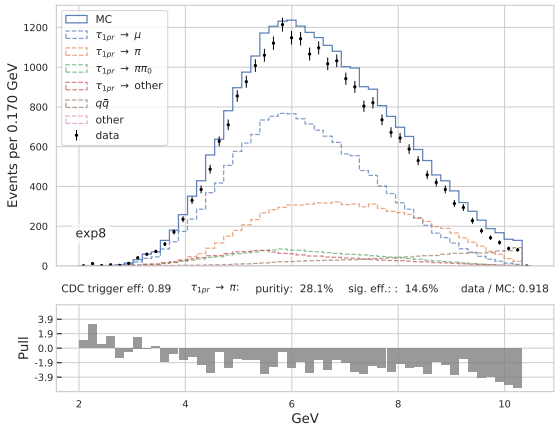

(d) visible energy CMS (π enriched sample)

Figure 7: Thrust and visible energy after background suppression.

3.3 Particle identification variables

One way to separate the π and μ is to look at particle identification (PID) variables like the muon identification probability (muonID) defined as

$$\mathsf{muonID} = \frac{\mathcal{L}_\mu}{\sum_i \mathcal{L}_i}$$

where $i \in \{e, \mu, \pi, K, p, d\}$. It takes information from all available detectors and calculates likelihood values $\mathcal{L}$ based on this information.

By requiring muonID > 0.5 for the μ sample the purity in MC gets increased to 89 % (see Figure 8a and Figure 8b). For the π sample we veto muons and electrons with muonID < 0.2 and electronID < 0.2. This increases purity to 63 % (see Figure 8c and Figure 8d).

A problem with using PID variables is that their distributions in data and MC do not match and a requirement on PID introduces a discrepancy between data and MC that can not be corrected reliably because MC is not fully calibrated yet. By comparing Figure 8a and Figure 8c one can see that for the μ sample the data / MC ratio went down, while for the π sample it went up. This reflects the data / MC distributions in muonID (Figure 9). Note that not only the scaling of the MC distribution can be affected, but their shape as well.

In Section 5 BF calculations are done for samples with and without using PID variables respectively.

3.4 Trigger

Because it is impossible to process and store detector information for all collisions there exists a trigger system which identifies events which are of interest for analysis. Therefore when comparing data with Monte Carlo one has to account for inefficiencies in the trigger system, since the trigger is not simulated in MC. One way to estimate the trigger efficiency from data is by looking at two triggers whose probability of being activated is completely uncorrelated. This way one trigger can serve as a reference and by looking at the subset of events where it was fired the efficiency for the other trigger can be estimated. This approach is called tag and probe (T&P).

For this Analysis the two triggers selected to calculate the T&P efficiencies are the *fff* and the *hie* trigger because they are expected to have a high efficiency and most of our signal events will satisfy the conditions for the trigger to be fired. The condition for the *fff* trigger to be fired is to detect more than two 2D tracks and no KEKB injection veto is present. The condition for the *hie* trigger to be fired is that the total energy deposited in the ECL is greater than 1 GeV and no Bhabha veto as well as no no KEKB injection veto is present. A Bhabha veto is applied if there are two high energy back to back cluster in the ECL. These triggers can be considered orthogonal because they take information from different parts of the detector, the *fff* trigger from the central drift chamber (CDC) and the *hie* trigger from the ECL. From now on I will refer to them as CDC and ECL trigger respectively.

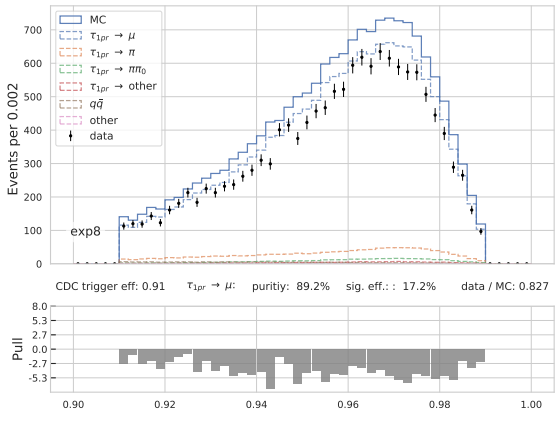

(a) thrust (μ sample)

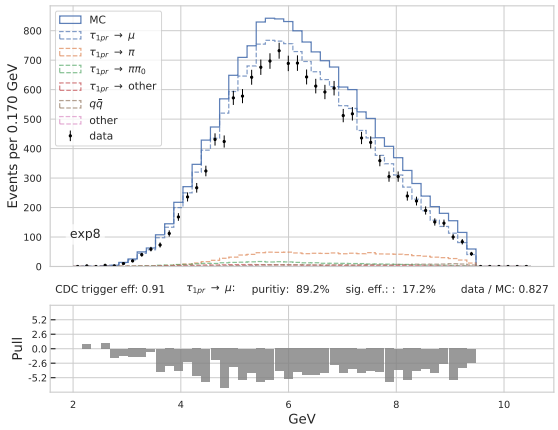

(b) visible energy CMS (μ sample)

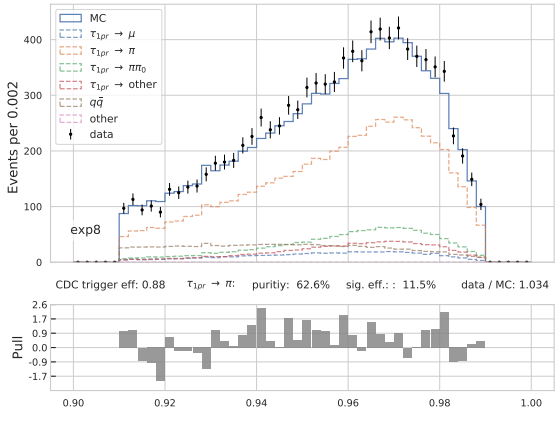

(c) thrust (π sample)

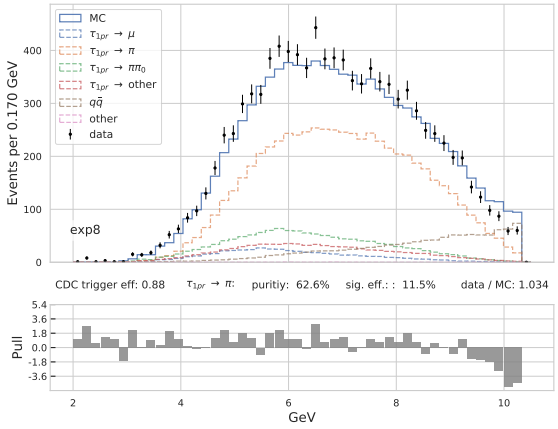

(d) visible energy CMS (π sample)

Figure 8: Thrust and visible energy after using PID varibles.

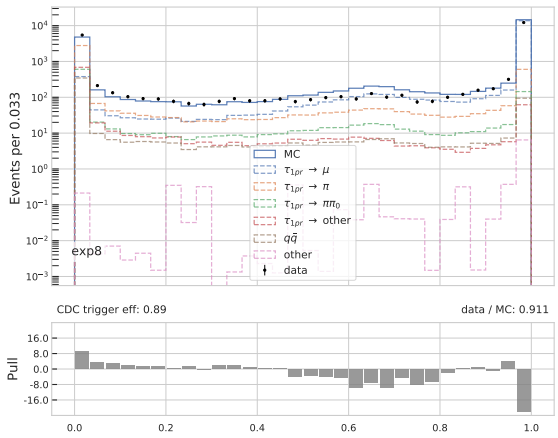

(a) muonID for μ sample

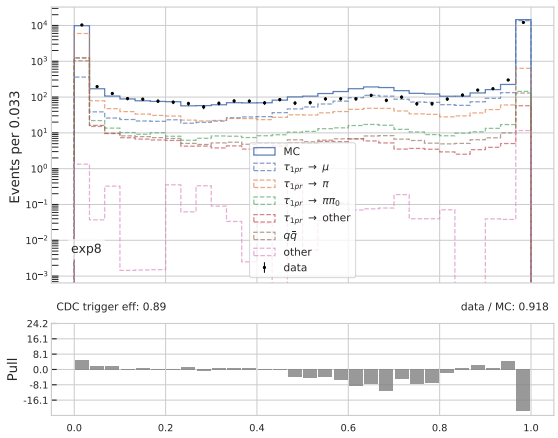

(b) muonID for π sample

Figure 9: Data / MC comparison for the muonID variable.

signal	$\epsilon_{\text{trig}}^{\text{ECL}}$	$\epsilon_{\text{trig}}^{\text{CDC}}$	$N_{\text{data}}^{\text{ECL}}$	$N_{\text{data}}^{\text{CDC}}$
$\tau_{1pr} \to \mu$	$(73.9 \pm 0.3)\,\%$	$(89.0 \pm 0.2)\,\%$	17 203	20 725
$\tau_{1pr} \to \mu$	$(73.5 \pm 0.4)\,\%$	$(90.5 \pm 0.3)\,\%$	11 316	13 934
$\tau_{1pr} \to \pi$	$(78.4 \pm 0.3)\,\%$	$(88.7 \pm 0.2)\,\%$	22 373	25 300
$\tau_{1pr} \to \pi$	$(84.5 \pm 0.4)\,\%$	$(87.9 \pm 0.3)\,\%$	9592	9984

Table 5: Trigger efficienceis for the different samples.

The trigger efficiencies will be calculated with

$$\epsilon_{fff}^{\text{T\&P}} = \frac{N_{fff} \wedge N_{hie}}{N_{hie}} \qquad \epsilon_{hie}^{\text{T\&P}} = \frac{N_{fff} \wedge N_{hie}}{N_{fff}}. \tag{5}$$

In Figure 10 the activation curve for the ECL trigger and the efficiency for the CDC trigger as a function of kinematics can be seen. The ECL trigger has close to 100% efficiency for events with total cluster energy greater than 1.5 GeV and the CDC trigger has higher efficiency if all tracks have a high transverse momentum.

The efficiency of the CDC trigger depends on the angle θ the individual tracks enclose with the beam axis. As shown in Figure 10c if a track (here shown for the 1-prong track) is on a trajectory with high or low θ the efficiency is very low. If we require all 4 tracks to be inside the CDC region ($-0.625 < \cos\theta < 0.846$) and look again at the efficiency of these events as a function of the smallest transverse momentum we can see the efficiency now having a plateau close to 1 (Figure 10d). The condition of all tracks to be in the barrel is only met by about 52% of all events.

The trigger efficiency is used to scale the MC distributions down while for data only the events are selected where the trigger fired. In this analysis I will use the CDC trigger since it has a higher efficiency and there are more data events that fire the trigger (see Table 5).

4 Template fit

To estimate the amount of signal in data we rely on information coming from MC. To neglect scaling errors in MC one approach is to scale the total MC exactly to data and then assume the fraction for the signal in MC to be the same as in data. To do this the number of data events can be simply multiplied by the purity. This is a good method if there exists just a global scaling error.

Another approach is to do a template fit. Here a probability density function (PDF) for the signal and different backgrounds is defined using histograms from MC. These PDFs can be fitted to data with floating normalization. This way not only global scaling errors but also errors for the individual processes can be accounted for. For this method to be effective the distributions for the individual processes should not be similar.

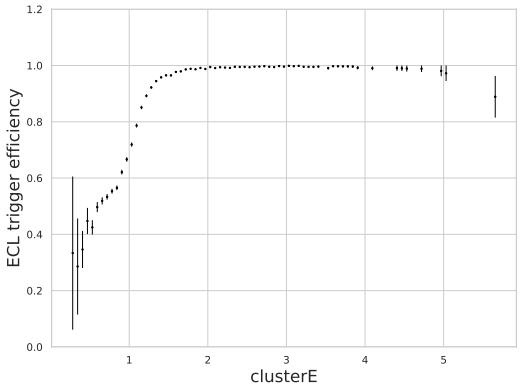

(a) ECL trigger efficiency as function of cluster energy.

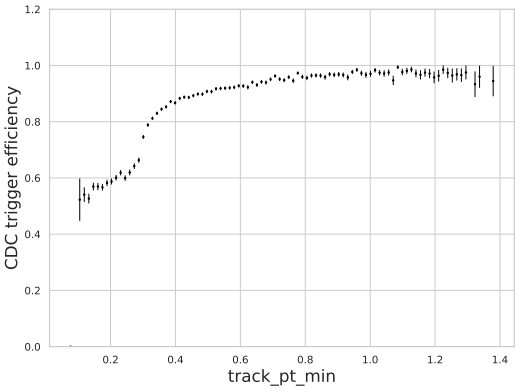

(b) CDC trigger efficiency as function of smallest transverse momentum.

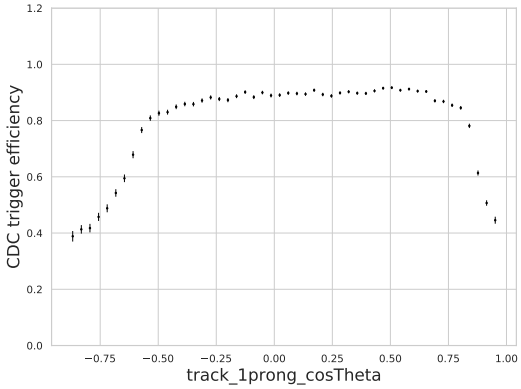

(c) CDC trigger efficiency as function of 1-prong track $\cos\theta$.

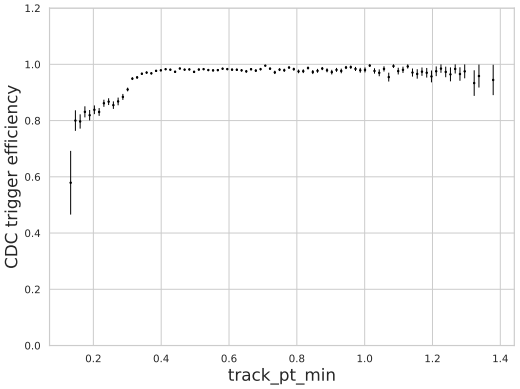

(d) CDC trigger efficiency with all tracks in the barrel.

Figure 10: Trigger efficiencies in dependence on some variables.

For my template fit I used the center of mass energy on the 1-prong side (ECMS_1prong) and the cosine of the angle of the track to the thrust vector. I divided my MC in 6 categories ($\tau_{1pr} \to \mu$, $\tau_{1pr} \to \pi$, $\tau_{1pr} \to \pi\pi_0$, $\tau_{1pr} \to$ other, $q\bar{q}$, other) and created a PDF for each category using a 2-dimensional histogram with 25 bins in each dimension. The distributions can be seen in Figure 11, here for the π sample without PID cuts. Bins are only taken into account for the fit if there are at least 10 data events in the bin. The white line indicates which bins are used for the fit. For the π sample the total number of bins used is 72.

The results of the template fit can be found in Table 6, Table 7, Table 8 and Table 9.In Figure 12 the fit results are shown as a projection onto ECMS 1prong and cos to thrust variables with data superimposed.

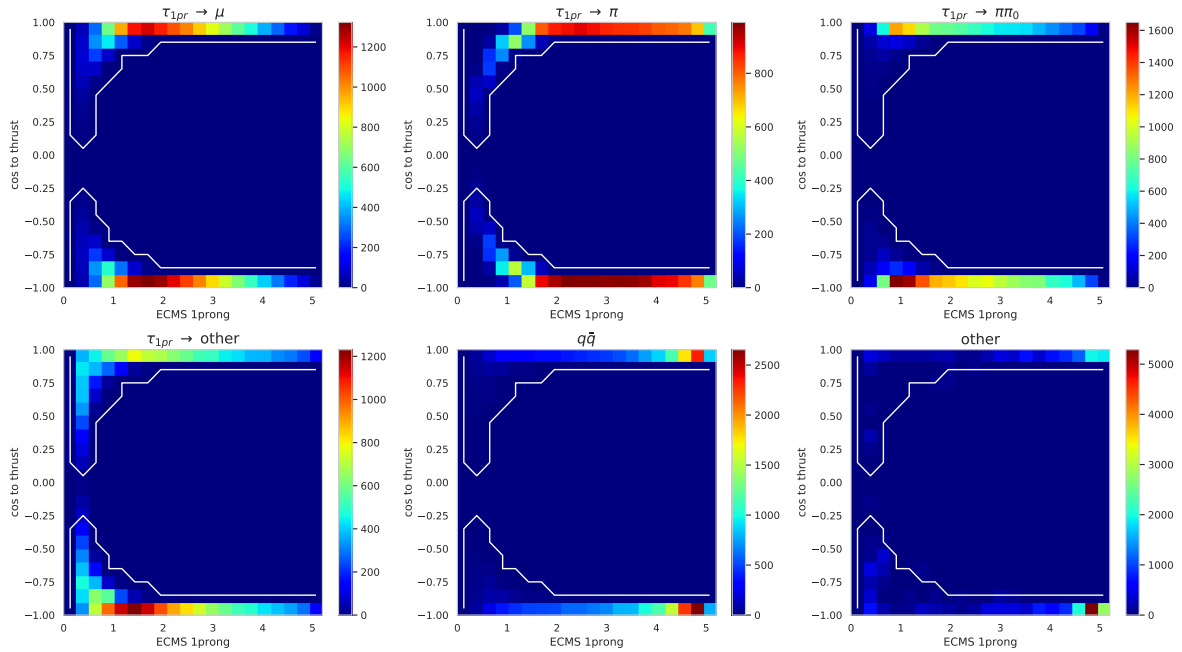

Figure 11: 2D binned PDFs for each category using the π sample.

channel	fraction of Data after fit	purity in MC	ratio
$\tau_{1pr} \to \mu$	$(71.10 \pm 2.21)\%$	$(68.78 \pm 0.05)\%$	(1.03 ± 0.03)
$\tau_{1pr} \to \pi$	$(17.53 \pm 1.56)\%$	$(19.53 \pm 0.04)\%$	(0.90 ± 0.08)
$\tau_{1pr} \to \pi\pi_0$	$(4.92 \pm 1.62)\%$	$(4.84 \pm 0.02)\%$	(1.02 ± 0.33)
$\tau_{1pr} \to$ other	$(3.96 \pm 0.81)\%$	$(4.17 \pm 0.02)\%$	(0.95 ± 0.19)
$q\bar{q}$	$(2.19 \pm 1.40)\%$	$(2.64 \pm 0.02)\%$	(0.83 ± 0.53)
other	$(0.00 \pm 0.57)\%$	$(0.04 \pm 0.01)\%$	(0.00 ± 14.27)
sum	$(99.70 \pm 0.72)\%$	100 %	

Table 6: Results of the template fit for the μ sample.

channel	fraction of Data after fit	purity in MC	ratio
$\tau_{1pr} \to \mu$	$(58.16 \pm 2.53)\%$	$(55.17 \pm 0.04)\%$	(1.05 ± 0.05)
$\tau_{1pr} \to \pi$	$(27.23 \pm 1.66)\%$	$(28.13 \pm 0.04)\%$	(0.97 ± 0.06)
$\tau_{1pr} \to \pi\pi_0$	$(6.98 \pm 1.71)\%$	$(6.33 \pm 0.02)\%$	(1.10 ± 0.27)
$\tau_{1pr} \to$ other	$(4.34 \pm 0.92)\%$	$(5.33 \pm 0.02)\%$	(0.81 ± 0.17)
$q\bar{q}$	$(3.00 \pm 1.11)\%$	$(5.00 \pm 0.02)\%$	(0.60 ± 0.22)
other	$(0.00 \pm 0.53)\%$	$(0.06 \pm 0.00)\%$	(0.00 ± 9.52)
sum	$(99.71 \pm 0.72)\%$	100 %	

Table 7: Results of the template fit for the π sample.

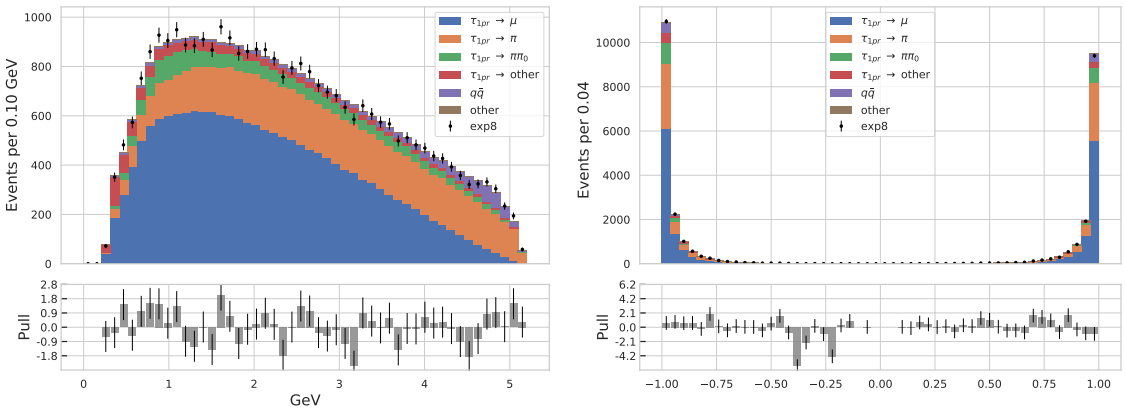

(a) 1-prong ECMS

(b) cos to thrust

Figure 12: Fit results projected on one dimension.

channel	fraction of Data after fit	purity in MC	ratio
$\tau_{1pr} \to \mu$	$(95.72 \pm 1.94)\%$	$(89.16 \pm 0.04)\%$	(1.07 ± 0.02)
$\tau_{1pr} \to \pi$	$(3.73 \pm 1.39)\%$	$(6.93 \pm 0.03)\%$	(0.54 ± 0.20)
$\tau_{1pr} \to \pi\pi_0$	$(0.00 \pm 1.88)\%$	$(2.01 \pm 0.02)\%$	(0.00 ± 0.93)
$\tau_{1pr} \to$ other	$(0.00 \pm 1.86)\%$	$(0.83 \pm 0.01)\%$	(0.00 ± 2.24)
$q\bar{q}$	$(0.00 \pm 1.49)\%$	$(1.02 \pm 0.01)\%$	(0.00 ± 1.46)
other	$(0.18 \pm 0.40)\%$	$(0.05 \pm 0.01)\%$	(3.76 ± 8.68)
sum	$(99.62 \pm 0.86)\%$	100 %	

Table 8: Results of the template fit for the μ sample with PID cuts.

channel	fraction of Data after fit	purity in MC	ratio
$\tau_{1pr} \to \mu$	$(6.56 \pm 2.01)\%$	$(4.94 \pm 0.03)\%$	(1.33 ± 0.41)
$\tau_{1pr} \to \pi$	$(61.87 \pm 1.99)\%$	$(62.56 \pm 0.07)\%$	(0.99 ± 0.03)
$\tau_{1pr} \to \pi\pi_0$	$(12.98 \pm 2.67)\%$	$(13.27 \pm 0.05)\%$	(0.98 ± 0.20)
$\tau_{1pr} \to$ other	$(12.46 \pm 4.93)\%$	$(8.23 \pm 0.04)\%$	(1.51 ± 0.60)
$q\bar{q}$	$(5.55 \pm 1.31)\%$	$(10.98 \pm 0.05)\%$	(0.51 ± 0.12)
other	$(0.00 \pm 0.37)\%$	$(0.01 \pm 0.01)\%$	(0.00 ± 25.52)
sum	$(99.41 \pm 1.09)\%$	100 %	

Table 9: Results of the template fit for the π sample with PID cuts.

sample	ϵ_{sig}	p_{fit}	p_{mc}
μ	$(18.24 \pm 0.09)\,\%$	$(71.1 \pm 2.2)\,\%$	$(68.78 \pm 0.05)\,\%$
μ_{pid}	$(17.23 \pm 0.08)\,\%$	$(95.7 \pm 1.9)\,\%$	$(89.16 \pm 0.04)\,\%$
π	$(14.58 \pm 0.09)\,\%$	$(27.2 \pm 1.7)\,\%$	$(28.13 \pm 0.04)\,\%$
π_{pid}	$(11.46 \pm 0.07)\,\%$	$(61.9 \pm 2.0)\,\%$	$(62.56 \pm 0.07)\,\%$

Table 10: Important parameters for BF calculation.

signal	$\mathcal{B}_{\mathsf{fit}}$	$\mathcal{B}_{\mathsf{fit}}/\mathcal{B}_{\mathsf{pdg}}$	$\mathcal{B}_{\mathsf{mc}}$	$\mathcal{B}_{\mathsf{mc}}/\mathcal{B}_{\mathsf{pdg}}$
$\tau_{1pr} \to \mu$	$(16.37 \pm 0.53)\,\%$	0.94 ± 0.03	$(15.84 \pm 0.12)\,\%$	0.91 ± 0.01
$\tau_{1pr} \to \mu_{\mathsf{pid}}$	$(15.43 \pm 0.35)\,\%$	0.89 ± 0.02	$(14.38 \pm 0.13)\,\%$	0.83 ± 0.01
$\tau_{1pr} \to \pi$	$(9.62 \pm 0.59)\,\%$	0.89 ± 0.05	$(9.94 \pm 0.08)\,\%$	0.92 ± 0.01
$\tau_{1pr} \to \pi_{\mathsf{pid}}$	$(11.07 \pm 0.38)\,\%$	1.02 ± 0.03	$(11.19 \pm 0.13)\,\%$	1.03 ± 0.01

Table 11: Calculated branching fractions for different samples.

5 BF calculation

To calculate the branching fraction we use

$$\mathcal{B}_{\mathsf{sig}} \approx \frac{N_{\mathsf{sig}}^{\mathsf{data}}}{2 \cdot \sigma_{\tau\tau} \cdot L^{\mathsf{data}} \cdot \mathcal{B}_{\mathsf{tag}} \cdot \epsilon_{\mathsf{trig}} \cdot \epsilon_{\mathsf{sig}}}, \tag{6}$$

where N_{sig} is the total number of signal events in data, ϵ_{trig} is the trigger efficiency and ϵ_{sig} is the signal efficiency calculated from Monte Carlo. N_{sig} will be estimated using the results of the fit described in Section 4 as well as with purity taken from MC. In Table 10 all important values for the different samples are summarized. No systematic uncertainties were considered for the calculation of the BF, the error shown originates only from statistical uncertainties.

In Table 11 the calculated BF are shown as well as their ratio to the PDG value.

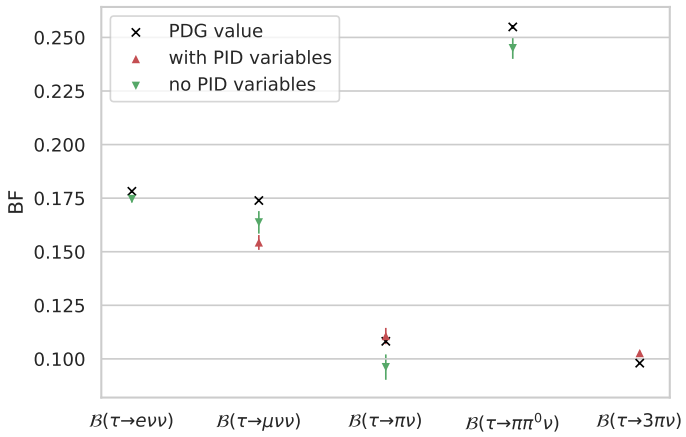

decay mode	Calculated value	with PID cuts	PDG value
$\tau \to e\nu\nu$	$(17.46 \pm 0.16)\%$		$(17.82 \pm 0.04)\%$
$\tau \to \mu\nu\nu$	$(16.37 \pm 0.53)\%$	$(15.43 \pm 0.35)\%$	$(17.39 \pm 0.04)\%$
$\tau \to \pi\nu$	$(9.62 \pm 0.59)\%$	$(11.07 \pm 0.38)\%$	$(10.82 \pm 0.05)\%$
$\tau \to \pi\pi^0\nu$	$(24.5 \pm 0.5)\%$		$(25.49 \pm 0.09)\%$
$\tau \to 3h\nu$		$(10.27 \pm 0.11)\%$	$(9.8 \pm 0.05)\%$

Figure 13: Calculated branching fractions compared to PDG values.

6 Conclusion

In my project I calculated the BF for the decays $\tau \to \mu\nu_\mu\nu_\tau$ and $\tau \to \pi\nu_\tau$ with and without using PID variables using a template fit to estimate the signal fraction from data as well as the purity. The signal efficiency was calculated only from MC, so the BF give a hint on PID performance and MC calibration. Additional information can be derived by comparing the BF for different decays. In Equation 6 we can see that by dividing two BF a lot of uncertainty afflicted values cancel. What is left is essentially the ratio of the number of signal events in data and the ratio of the efficiencies. ϵ_{sig} is actually a product of many efficiencies (originating from detection, reconstruction and selection), some of which will also cancel. This way performances can be estimated by comparing the BF ratio to the value calculated from PDG.

Three other students estimated the BF for $\tau \to e\nu\nu$, $\tau \to \pi\pi^0\nu$ and $\tau \to 3h\nu$ doing a similar analysis. Their results together with my values (using the template fit) are listed and visualized in Figure 13.

In Figure 14 some ratios of the BF (using the template fit) are listed. In Figure 14a the BF ratios normalized to the PDG ratios are visualized. In Figure 14b the same is shown for BF calculated using purity from MC instead of the template fit.

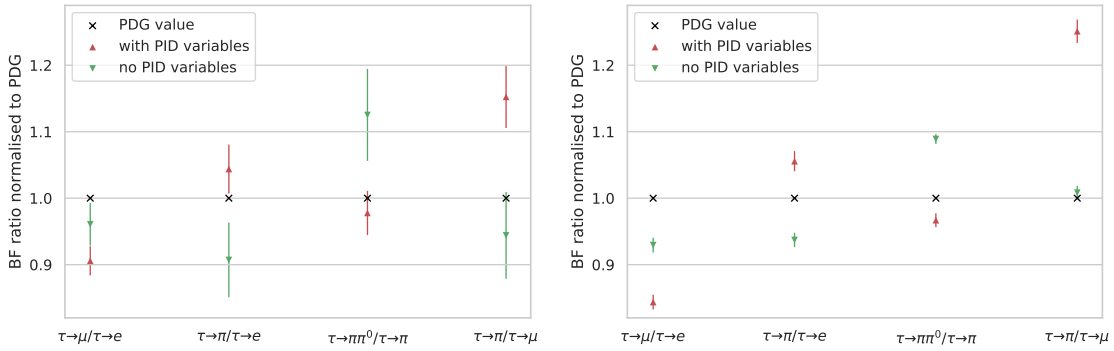

(a) using results of the template fit

(b) using only purity from MC

Ratio of BFs	Calculated value	with PID cuts	PDG value
$\mathcal{B}(\tau \to \mu\nu\nu)$ / $\mathcal{B}(\tau \to e\nu\nu)$	0.94 ± 0.03	0.88 ± 0.02	0.976 ± 0.003
$\mathcal{B}(\tau \to \pi\nu)$ / $\mathcal{B}(\tau \to e\nu\nu)$	0.55 ± 0.03	0.63 ± 0.02	0.607 ± 0.003
$\mathcal{B}(\tau \to \pi\pi^0\nu)$ / $\mathcal{B}(\tau \to \pi\nu)$	2.55 ± 0.17	2.21 ± 0.09	2.356 ± 0.014
$\mathcal{B}(\tau \to \pi\nu)$ / $\mathcal{B}(\tau \to \mu\nu\nu)$	0.59 ± 0.04	0.72 ± 0.03	0.622 ± 0.003

Figure 14: Branching fraction ratio comparison (normalised to PDG values).

With increased MC calibration and more data a goal for the future is to calculate the BF purely from data and test the standard model prediction with high precision.